Inhibitors of the ubiquitin-proteasome system rescue cellular levels and ion transport function of pathogenic pendrin (SLC26A4) protein variants

EMANUELE BERNARDINELLI[1], RAPOLAS JAMONTAS[1], ARNOLDAS MATULEVIČIUS[1], FLORIAN HUBER[1], HOUSSEIN NASSER[1], SOPHIE KLAUS[1], HAIXIA ZHU[2], JIANGANG GAO[2] and SILVIA DOSSENA[1,3]

[1]Institute of Pharmacology and Toxicology, Paracelsus Medical University, A-5020 Salzburg, Austria; [2]Institute of Developmental Biology, School of Life Science, Shandong University, Qingdao, Shandong 266237, P.R. China; [3]Research and Innovation Center Regenerative Medicine and Novel Therapies (FIZ RM&NT), Paracelsus Medical University, A-5020 Salzburg, Austria

Received October 8, 2024; Accepted February 18, 2025

DOI: 10.3892/ijmm.2025.5510

Abstract. Pendrin (SLC26A4) is an anion exchanger abundantly expressed in the inner ear, kidney and thyroid, and its malfunction resulting from genetic mutation leads to Pendred syndrome and non-syndromic deafness DFNB4. Pathogenic variants of the pendrin protein are less expressed than the wild-type, but the mechanism underlying this phenomenon is unknown. In the present study, the hypothesis that reduced protein expression stems from increased protein degradation was explored. To verify this hypothesis, the protein levels and anion transport function of several pathogenic pendrin variants were measured following exposure to inhibitors of the ubiquitin-proteasome system (UPS) and the lysosomal/autophagosomal pathways. Protein levels were measured by western blotting and quantitative imaging; ion transport was measured with a fluorometric method. Post-translational modification of pendrin was investigated by immunoprecipitation and mass spectrometry. The results showed that the protein abundance and half-life of pathogenic pendrin variants were significantly reduced compared with the wild-type in cell-based assays and in a mouse model of Pendred syndrome/DFNB4, pointing to accelerated protein degradation rather than defective protein production. Wild-type pendrin and its variants are abundantly but differentially ubiquitinated, consistent with their different protein stability. While ubiquitination at the C-terminus controls the stability of wild-type pendrin, preferential ubiquitination of lysine 77 occurred in the pathogenic pendrin variant p.R409H. Inhibition of the UPS with investigational (MG132) or clinical (bortezomib, delanzomib, or carfilzomib) proteasome inhibitors rescued the expression, plasma membrane targeting, and ion transport function of pathogenic pendrin variants, while inhibition of the lysosomal/autophagosomal pathway was ineffective. Among the compounds tested, carfilzomib rescued the ion transport of pendrin p.R409H to wild-type levels. These findings suggest that targeting specific molecular players within the UPS can rescue the expression and activity of pathogenic variants of the pendrin protein, which represents a novel therapeutic concept for Pendred syndrome/DFNB4.

Correspondence to: Dr Silvia Dossena, Institute of Pharmacology and Toxicology, Paracelsus Medical University, Strubergasse 21, A-5020 Salzburg, Austria
E-mail: silvia.dossena@pmu.ac.at

Abbreviations: CFTR, cystic fibrosis transmembrane conductance regulator; DFNB4, deafness autosomal recessive 4; ECFP, enhanced cyan fluorescent protein; EVA, enlarged vestibular aqueduct; ER, endoplasmic reticulum; EYFP, enhanced yellow fluorescent protein; MS, mass spectrometry; LC-MS/MS, liquid chromatography-tandem MS; UPS, ubiquitin-proteasome system

Key words: ion transport, pathogenic variants, pendrin, SLC26A4, UPS, UPS inhibitors

Introduction

Pendrin (SLC26A4) is an electroneutral exchanger for monovalent anions that is expressed on the apical membrane of distinct epithelial cells in several tissues (1-4). In the inner ear, the physiological functions of pendrin are complex and include the modification of the ion composition, pH and volume of the endolymph. Specifically, Cl^- reabsorption linked to a pendrin-dependent Cl^-/HCO_3^- exchange residing on the mitochondria-rich cells permits fluid reabsorption in the endolymphatic sac, thereby controlling the volume of the endolymph (5). In the cochlea, HCO_3^- secretion from pendrin-expressing non-sensory cells prevents acidification of the endolymph and is fundamental in the maintenance of endolymphatic ion homeostasis (6,7). In the thyroid, pendrin contributes to the transport of iodide into the colloidal lumen of thyroid follicles, most likely via a Cl^-/I^- exchange (8). In the kidney, pendrin is part of the molecular machinery of beta-intercalated cells that, in the distal nephron, reacts to metabolic alkalosis by activating HCO_3^- secretion into the pre-urine. Simultaneously, pendrin drives a Cl^- reabsorption that permits salt and fluid reabsorption and contributes to controlling systemic blood pressure (9-11).

Genetically determined loss of pendrin function in humans leads to isolated autosomal recessive deafness B4 (DFNB4, OMIM ID_600791) and Pendred syndrome, which is defined as the association between hearing loss and thyroid dysfunction due to a defective iodide organification (OMIM ID_274600) (12,13). The clinical course of hearing loss varies among subjects with Pendred syndrome/DFNB4. Some patients lose hearing during their early childhood, which severely compromises language onset and discrimination. However, other patients manifesting fluctuating and progressive or sudden hearing loss lose hearing later in life (14). Hearing loss in Pendred syndrome/DFNB4 is consistently associated with a malformation of the temporal bone called enlarged vestibular aqueduct (EVA), while a cochlear incomplete partition type II (Mondini cochlea) may or may not be present. The findings of ears with EVA and normal hearing indicate that EVA does not directly cause hearing loss but can be considered a radiologic marker of the genetic etiology of this condition (14,15).

Ablation of the *Slc26a4* gene in the mouse was instrumental in clarifying the pathological mechanism of pendrin-related hearing loss. The most striking findings in pendrin knockout mice are profound deafness and prominent enlargement of all inner ear compartments, including the *scala media* of the cochlea and the endolymphatic sac and duct (16,17). Hearing loss in these mice appears to be the consequence of sequential and probably causally connected perturbations of the ion and volume homeostasis of the endolymph, starting with acidification of the cochlear endolymph due to lack of pendrin-dependent bicarbonate secretion and expansion of the endolymphatic compartment due to lack of pendrin-driven salt and fluid reabsorption in the endolymphatic sac. The cochlear fluid expansion was suggested to lead to metabolic stress in the *stria vascularis* due to an increased rate of K^+ secretion, with loss of expression of the oxidative stress-sensitive K^+ channel KCNJ10/Kir4.1 and consequential loss of endo-cochlear potential (7). Both the loss of the endo-cochlear potential, which is positive in the lumen of the *scala media*, and inhibition of the pH-sensitive Ca^{++} channels TRPV5/TRPV6, would cause an increase in the endolymphatic Ca^{2+} concentration, ultimately leading to the degeneration of the sensory hair cells in the organ of Corti (17,18). These derangements point to the dysregulation of ion transport as a key pathogenic factor in Pendred syndrome/DFNB4. Therefore, a potential therapeutic approach should aim to recover the ion transport function of pathogenic pendrin variants.

Studies in transgenic mice where pendrin expression could be induced and terminated at defined time points revealed that the time window between embryonic day 16.5 and post-natal (P) day 2 is critical for hearing acquisition (15). Importantly, induction of pendrin expression at P6 stabilized hearing in a mouse model of fluctuating and progressive hearing loss with EVA (19). These findings indicate that interventions to recover pendrin expression during the pre-natal or early post-natal phase may have therapeutic potential in Pendred syndrome/DFNB4 (17). Interestingly, while pendrin knockout mice invariably exhibit profound deafness, in our pendrin p.L236P knock-in mouse the degree of hearing loss varies from mild to profound, more closely resembling the human phenotype (20). Together, these considerations support the existence of a temporal window of possible intervention to prevent hearing loss or protect and stabilize residual hearing in patients with Pendred syndrome/DFNB4. However, no mechanistic approaches toward these therapeutic goals have been developed.

The great majority of inherited alterations of the *SLC26A4* gene lead to the production of pathogenic protein variants with a single amino acid substitution. Seminal studies of these pendrin variants in heterologous expression systems helped reveal the pathological mechanism of disease. Pathogenic pendrin variants showed a partial or total impairment of ion transport activity, which was initially associated with misfolding of the protein, retention within intracellular compartments, and consequential failure in reaching the cell surface (21,22). Later, studies revealed that several pendrin variants, although compromised concerning their ion transport ability, are correctly expressed at the plasma membrane (23-27). Importantly, it was found out that reduction of total protein expression, rather than mis-localization, appears to be a key feature of all functionally impaired pendrin variants (26,27).

Very little is known about the mechanisms controlling the protein levels of wild-type pendrin and its variants. Misfolded cellular proteins undergo ubiquitination and ubiquitin-proteasome system (UPS)-mediated degradation. It was previously shown that the fusion protein wild-type pendrin-GFP is a slow-folding protein that accumulates in the endoplasmic reticulum (ER) and perinuclear aggregates and is ubiquitinated (28), but the ubiquitination sites remained unknown. The ER membrane-associated ubiquitin ligase Rma1 was identified as a regulator of the cellular levels of wild-type and p.H723R pendrin, but not those of p.L236P and other variants (29). Interestingly, in conditions of blockade of the ER-to-Golgi transit or ER stress, the misfolded pendrin p.H723R can bypass the Golgi, reach the plasma membrane, and exhibit significant ion transport function. This phenomenon depends on the heat shock cognate protein 70 (Hsc70) and the HSP70 co-chaperone DNAJC14 (30). Ubiquitination not only determines protein degradation but also controls subcellular localization. The E3 HECT ubiquitin ligase Nedd4-2 controls the trafficking of wild-type pendrin at the apical membrane of beta-intercalated cells in the mouse cortical collecting duct and connecting tubule, with no major influence on the total protein abundance (31).

In the present study, it was demonstrated that the cellular expression levels of wild-type pendrin and its pathogenic protein variants are controlled by the UPS, and UPS inhibitors can rescue pendrin protein expression and function.

Materials and methods

Mammalian expression vectors. The pTARGET (Promega Corporation) vector coding for human SLC26A4 (NCBI Sequence ID: NM_000441.2) with or without a hexa-histidine tag at the C-terminus was used for transfecting cells for functional testing and some of the western blotting, respectively. For functional testing, the enhanced yellow fluorescent protein (EYFP) pEYFPN1 p.H148Q;I152L plasmid was also used. This vector encodes for the EYFP variant p.H148Q;I152L, which is sensitive to the intracellular iodide concentration (32). The pFLAG-CMV-4 (Sigma-Aldrich; Merck KGaA) vector

coding for SLC26A4 with a Met-FLAG tag at the N-terminus was used for transfecting cells for immunoprecipitation, half-life measurements, and western blotting.

For the determination of pendrin expression levels via quantitative imaging, cells were transfected with the pEYFPN1 vector (Takara Bio USA, Inc.) to produce pendrin with the EYFP fused to its C-terminus (SLC26A4-EYFP). In experiments where the plasma membrane expression was evaluated, cells were co-transfected with equimolar amounts of the SLC26A4-EYFP vector and a vector coding for the enhanced cyan fluorescent protein (ECFP) (pECFPC1 vector; Takara Bio USA, Inc.).

Sequence alterations in the pendrin coding sequence were performed using the QuikChange® site-directed mutagenesis kit (Agilent Technologies, Inc.) according to the manufacturer's protocol using the following primers: p.L236P forward, 5'-GCTGGTCTCACAGCCAAAGATTGTCCTCAATG-3' and reverse, 5'-CATTGAGGACAATCTTTGGCTGTGAGACCAGC-3'; and p.R409H forward, 5'-ACTGCTCTTTCCCACACGGCCGTCCAGGA-3' and reverse, 5'-TCCTGGACGGCCGTGTGGGAAAGAGCAGT-3'. The plasmid vectors coding the other pendrin variants have already been described (26). Sequential C-terminal SLC26A4 truncations were obtained by inserting a STOP codon at the appropriate nucleotide position in the SLC26A4 sequence into the pFLAG-CMV-4 vector. The integrity of all coding sequences was verified by Sanger sequencing (Microsynth AG).

Animals. Homozygous mutant mice bearing the Slc26a4 variant p.L236P were generated using the CRISPR/Cas9 genome editing technology and have been previously described (20). The animals were kept in a standard environment with a temperature of 22±1˚C and a relative humidity of 50-60%, and they were allowed free access to food and water. The age of the mice used in the present study was 2-3 months-old and weighed >20 g. Mice were euthanized by cervical dislocation. Each group of experiments involved 3 male mice. The treatment of all the animals was in strict accordance with the requirements of animal experiments at Shandong University (Jinan, China), which were approved by the Ethics Committee of the School of Life Science, Shandong University (approval no. SYDWLL-2021-76).

Reverse-transcription quantitative PCR (RT-qPCR). For RT-qPCR, total RNA was extracted from mouse kidneys with the TRIzol reagent (Invitrogen; Thermo Fisher Scientific, Inc.). Reverse transcription was conducted with SPARKscript II All-in-one RT SuperMix for qPCR with gDNA Eraser following the manufacturer's protocol (Shandong Sparkjade Scientific Instruments Co., Ltd.), and qPCR was made with 2X SYBR Green qPCR Mix with ROX (Shandong Sparkjade Scientific Instruments Co., Ltd.). For qPCR, the initial denaturation temperature was 95˚C, followed by 30 cycles of denaturation (95˚C, 30 sec), annealing (60˚C, 30 sec) and extension (72˚C, 30 sec). The Bio-Rad Sequence Detection System (Bio-Rad Laboratories Inc.) was used to detect the expression levels of *Slc26a4*. The primers used were as follows: *Slc26a4* forward, 5'-AAGAGAGCCTTTGGTGTGGTA-3' and reverse, 5'-CAGGGCATAAGCCATCCCTTG-3'; and *ACTB* forward, 5'-GGCTGTATTCCCCTCCATCG-3' and reverse, 5'-CCAGTTGGTAACAATGCCATGT-3'. Relative gene expression values were quantified using the comparative Ct method (33).

Cell transfection. 293 Phoenix cells (34) (EcoPhoenix, https://ngvbcc.org/ReagentRepositoryView?prefillSearch=Cell%20Line), a highly transfectable derivative of 293T cells (CVCL_0063), were a kind gift from Prof. M. Baruscotti from the University of Milan (Italy). HeLa cells (human cervical adenocarcinoma, CCL-2) were directly obtained from the American Type Cell Culture Collection. These cells were cultivated as previously described (26,27). 293 Phoenix cells were transfected with the calcium phosphate co-precipitation method for 48 h, and Hela cells were transfected with METAFECTENE PRO® (Biontex Laboratories GmbH) for 72 h. The ratio μg DNA: μl METAFECTENE PRO® was 1:2.

For western blotting, confocal imaging, half-life measurements, and immunoprecipitation, cells were seeded into six-well plates and transfected with 3 μg/well (293 Phoenix) or 1.5 μg/well (HeLa) of the indicated plasmids. After 6-8 h, the transfection medium was replaced with a fresh medium.

For functional testing, 293 Phoenix cells were seeded into black 96-well plates and co-transfected with 0.12 μg/well of the pTARGET plasmid encoding for wild-type pendrin or its variants and 0.12 μg/well of the EYFP p.H148Q; I152L plasmid. The endogenous iodide influx was determined in cells co-transfected with 0.12 μg/well of the EYFP p.H148Q; I152L vector and 0.12 μg/well of the empty pTARGET vector. The background fluorescence was measured in cells transfected with 0.24 μg/well of the pTARGET vector.

Pendrin functional test. The ion transport function of pendrin was measured via a fluorometric method allowing for evaluation of iodide influx in cells transfected with pendrin and the iodide-sensitive fluorescent probe EYFP p.H148Q;I152L, as formerly described (26,27,35-42). Additional details are provided in Appendix S1.

Half-life measurements and western blotting. For pendrin half-life measurements, 293 Phoenix cells were seeded in 6-well plates and transfected with wild-type FLAG-SLC26A4 or the p.L236P and p.R409H variants. After transfection (24 h), the cells were treated with 25 μg/ml cycloheximide (Sigma-Aldrich; Merck KGaA) to block the protein synthesis and collected 0, 2, 4, 8 and 24 h after treatment. To assess the effect of proteasome inhibition with MG132, N-terminally flagged full-length pendrin and its C-terminal truncations were expressed in 293 Phoenix cells for 48 h and incubated with 1-10 μM MG132 or the vehicle (0.01% DMSO) for 16 h. To assess the effect of inhibition of the autophagosomal/lysosomal pathway, N-terminally flagged wild-type pendrin and its p.R409H or p.L236P variants were expressed in 293 Phoenix cells for 48 h and incubated with 200 μM chloroquine or the vehicle (water) for 6 h. Each cell pellet corresponding to one or two wells of a 6-well plate was lysed by resuspension in 50-100 μl RIPA buffer (Sigma-Aldrich; Merck KGaA) supplemented with 1X Halt Protease Inhibitor Cocktail (Thermo Fisher Scientific, Inc.) to obtain total proteins. Cell lysates were centrifuged at 900 x g for 10 min at 4˚C, and the supernatant was submitted to western blotting. Where indicated, whole cell lysates (20 μg total proteins) were submitted to deglycosylation

with 50,000 units/ml PNGase F (cat. no. P0704; New England Biolabs) for 24 h at 37˚C before western blotting.

To assess the effect of proteasome inhibition with MG132 on pendrin variants, 293 Phoenix cells were transfected for 48 h with wild-type pendrin or its variants and collected by centrifugation. The total membrane protein fraction was obtained with the Plasma Membrane Extraction kit (MBL International Corporation) and subjected to western blotting.

Western blotting was performed with standard methods. Additional details are given in Appendix S1. Pendrin detection was done with a mouse monoclonal anti-FLAG® M2 antibody (cat. no. F3165; Sigma-Aldrich; Merck KGaA) diluted 1:1,000 (half-life measurements) or with a rabbit anti-pendrin polyclonal antibody raised against amino acids 586-780 of human pendrin (cat. no. sc-50346; Santa Cruz Biotechnology, Inc.) diluted 1:500. The housekeeping proteins alpha-tubulin or calreticulin/calregulin were detected with mouse monoclonal antibodies (1:2,000; cat. no. 05-829; Sigma-Aldrich; Merck KGaA; or 1:100; cat. no. sc-373863; Santa Cruz Biotechnology, Inc.) and GAPDH was detected with a goat polyclonal antibody (1:1,000; cat. no. PLA0302; Sigma-Aldrich; Merck KGaA). The secondary antibodies (goat anti-rabbit, cat. no. 92632211; goat anti-mouse, cat. no. 926-32210; or donkey anti-goat, cat. no. 926-32214; conjugated to IRDye-800 CW, all from LI-COR Biosciences) were diluted 1:20,000. The signal of immunocomplexes was detected using the Odyssey (LI-COR Biosciences) infrared imaging system. Densitometric analysis was conducted using the ImageJ (1.53t) software (National Institutes of Health).

Western blotting on total proteins of mouse kidney was performed with a customized polyclonal antibody raised in rabbit against two partially overlapping synthetic peptides corresponding to the C-terminus of human pendrin (Davids Biotechnologie GmbH). The antibody was diluted (1:1,000) and membranes were blocked with 1% BSA (cat. no. 1.12018.0100; Sigma-Aldrich; Merck KGaA) in TBST (0.1% Tween 20) at room temperature for 2 h. β-actin was used as the housekeeping protein.

Total protein expression. Quantitative imaging to determine total protein expression was performed by confocal microscopy (Leica TCS SP5II AOBS; Leica Microsystems GmbH) as formerly described (26,27). The expression levels of wild-type or mutant SLC26A4-EYFP are given as the EYFP fluorescence intensity normalized for the cell density. Additional details are reported in Appendix S1.

Plasma membrane protein expression. The protein expression levels of wild-type or mutant SLC26A4-EYFP in the plasma membrane region were determined by confocal microscopy in live HeLa cells co-transfected with ECFP and stained with the CellMask™ Deep Red plasma membrane stain (cat. no. C10046; Molecular Probes; Thermo Fisher Scientific, Inc.) by using a formerly optimized protocol (26). The ECFP signal allowed normalization of the protein expression for the transfection efficiency of the single cell. Additional information is provided in Appendix S1.

Autophagosome staining and co-localization. Hela cells seeded in 6-well plates were transfected with 1.5 μg/well wild-type or mutant SLC26A4-EYFP plasmid vector and 3 μl/well METAFECTENE PRO® (cat. no. T040-2.0; Biontex Laboratories GmbH) at 37˚C, transferred on glass slides after 42 h, and incubated overnight with 100 μM chloroquine or the vehicle. The total transfection time was 72 h. After this, cells were fixed in 4% paraformaldehyde for 15 min, permeabilized with 0.2% Triton X-100, blocked with 3% BSA for 1 h at room temperature, incubated overnight with a rabbit polyclonal 1 μg/ml anti-LC3B antibody (cat. no. L10382; Invitrogen™; Thermo Fisher Scientific, Inc.; in 0.1% BSA), thoroughly washed, and incubated for 1 h at room temperature with a goat anti-rabbit Cy5®-conjugated IgG (cat. no. ab6564; Abcam) diluted 1:2,500 in 0.1% BSA. Finally, nuclei were counterstained with 0.1 μg/ml DAPI for 10 min, and cells were kept and imaged in PBS. Imaging was performed by sequential acquisition confocal microscopy. The imaging parameters were as follows: DAPI, excitation wavelength 405 nm (diode laser), emission range 450-490 nm. EYFP, excitation wavelength 514 nm (argon laser), emission range 525-600 nm; Cy5, excitation wavelength 633 nm (HeNe laser), emission range 650-750 nm. Co-localization between SLC26A4 (EYFP) and autophagosomes (Cy5) was quantified and expressed as Pearson's correlation coefficient by using the colocalization plugin of the LAS AF software (Leica Microsystems GmbH).

Cell viability tests. Cell proliferation was determined with the CellTiter 96® AQueous One Solution Cell Proliferation Assay system (Promega Corporation). Cells were seeded in 96-well plates, treated with proteasome inhibitors or their vehicle (DMSO) for 6-16 h, and incubated with 10 μl CellTiter 96® AQueous One Solution Reagent for 1.5 h in a humidified 5% CO_2 atmosphere. The formation of formazan was determined by reading the absorbance at 490 nm (VICTOR™ X3 Multilabel Plate Reader; Perkin Elmer, Inc.). All readings were corrected for the absorbance of the background.

To measure the cell density, cells were seeded in 24-well plates, treated with proteasome inhibitors or their vehicle, fixed in 4% paraformaldehyde for 30 min, stained with 0.1 μg/ml DAPI for 10 min, thoroughly washed, and kept in HBSS. The fluorescence of DAPI was read following excitation at 355 nm (VICTOR™ X3 Multilabel Plate Reader) and subtracted for the background fluorescence.

Immunoprecipitation and ubiquitination assay. 293 Phoenix cells seeded in 6-well plates were transfected for 48 h with wild-type or mutant FLAG-SLC26A4 or left untreated and collected by centrifugation. Each cell pellet corresponding to a whole 6-well plate was lysed in 300 μl Pierce™ IP Lysis Buffer (Thermo Fisher Scientific, Inc.) supplemented with 1X Halt Protease Inhibitor Cocktail (Thermo Fisher Scientific, Inc.). Cell lysates were centrifuged at 900 x g for 10 min at 4˚C, the supernatant was saved and the protein content was quantified. Total protein (1 mg) was incubated overnight at 4˚C with 10 μg of a mouse monoclonal anti-FLAG® M2 antibody (cat. no. F3165; Sigma-Aldrich; Merck KGaA) in 400 μl IP Lysis Buffer on a tube rotator. Subsequently, this sample was incubated with 50 μl Dynabeads™ Protein A (Invitrogen™; Thermo Fisher Scientific, Inc.) for 3 h at room temperature on a tube rotator. Beads were washed 3 times with 0.2% Tween-20 in PBS and eluted in 20 μl sample buffer containing 100 mM

dithiothreitol and 8% SDS. The eluates were boiled at 95˚C for 5 min and subjected to western blotting with anti-FLAG antibody (1:1,000 in 5% non-fat dry milk in TBST) to confirm the presence of pendrin in the immunoprecipitated samples. GAPDH (goat anti-GAPDH; 1:1,000; cat. no. PLA0302; Sigma-Aldrich; Merck KGaA) was detected to ensure the absence of unrelated cellular proteins in the immunoprecipitated samples. To detect ubiquitination, membranes were stripped and probed with a mouse monoclonal anti-ubiquitin antibody (P4D1; 1:1,000; cat. no. sc-8017; Santa Cruz Biotechnology, Inc.). In a subset of experiments, the immunoprecipitated proteins were subjected to deglycosylation by incubating the beads with 50,000 units/ml PNGase F (New England Biolabs) for 24 h at 37˚C.

Mass spectrometry (MS). For ubiquitination analysis by MS, 293 Phoenix cells were transfected with the pFLAG vector coding for wild-type pendrin or the pendrin variant p.R409H and incubated overnight with the proteasome inhibitor MG132 (1 μM; cat. no. C2211; Sigma-Aldrich; Merck KGaA) or its vehicle (0.01% DMSO). Protein extracts from cell lysates obtained in RIPA buffer were immunoprecipitated with an anti-FLAG antibody as described above, separated on a 9% acrylamide gel, and the band corresponding to pendrin (90-120 kDa) was cut from the gel. Trypsin digestion for the liquid chromatography-tandem mass spectrometry (LC-MS/MS) ubiquitination analysis was performed overnight at 37˚C directly on the gel slice. Peptides were extracted from the gel slice, lyophilized, and resuspended in 0.1% formic acid before the analysis. Peptides were separated in an Ultimate™ 3000 RSLCnano UHPLC system (Thermo Fisher Scientific, Inc.) with a flow rate of 250 nl/min. Additional details are given in Appendix S1. Raw MS output files were analyzed and searched against the human pendrin reference sequence (NP_000432.1) using Maxquant (1.6.2.6) in order to identify GlyGly-modified peptides. The analysis was performed in duplicate for both wild-type pendrin and the p.R409H variant, with and without MG132 treatment.

Salt and chemicals. Bortezomib (cat. no. PS-341), carfilzomib (cat. no. PR-171), delanzomib (cat. no. CEP-18770), ataluren (cat. no. PTC124), elexacaftor (cat. no. VX-445), lumacaftor (cat. no. VX-809) and tezacaftor (cat. no. VX-661) were obtained from Selleck Chemicals. MG132, tenidap (cat. no. PZ0196) and rapamycin (cat. no. 553211) were from Sigma-Aldrich; Merck KGaA. To prepare stock solutions, compounds were dissolved in dimethyl-sulfoxide (DMSO) (Sigma-Aldrich; Merck KGaA) and stored at -80˚C.

Correlation analysis and statistics. For the correlation analysis shown in Fig. 1, panels D-F, raw data for ion transport function, total protein abundance, and plasma membrane protein abundance of pendrin variants are obtained either from a previous study by the authors (26) (p.P142L, p.G149R, p.T193I, p.C282Y, p.Q413R, p.L445W and p.R776C) or from the present study (p.L236P and p.R409H). Ion transport function values have been subtracted for the endogenous iodide influx determined in cells transfected with the empty vector to obtain the net iodide influx of each variant. All data are expressed as a fraction of the wild-type (0-1). A positive correlation between data sets was tested by linear regression and expressed as Pearson's r coefficient.

Data are expressed as arithmetic mean ± standard error of the mean (S.E.M.). GraphPad Prism (version 10.2.3 for Mac OS, GraphPad Software, Inc.; Dotmatics) and Excel (Microsoft Corporation) software were used for statistical analysis and graphics generation. Significant differences between two or more data sets were determined by the one-sample or two-tailed unpaired Student's t-test or one-way or two-way ANOVA with Bonferroni´s, Dunnet's, or Tukey's post hoc test, as appropriate. $P<0.05$ was considered to indicate a statistically significant difference; (n) corresponds to the number of independent samples.

Results

Pathogenic variants of the pendrin protein undergo rapid cellular degradation. As aforementioned, it has been previously shown that reduction in protein expression is a common feature of pathogenic pendrin variants (26,27), but the underlying mechanisms remained unknown. To test whether reduced expression stems from accelerated protein degradation, the half-life of ectopically expressed wild-type pendrin and pendrin variants p.L236P and p.R409H, which are two of the most common pathogenic pendrin variants in Caucasians, was measured (43,44). The results clearly revealed that, after the block of the protein synthesis (time 0), pendrin protein abundance was significantly influenced by time ($P<0.0001$, two-way ANOVA) and variant type ($P<0.0001$). In addition, there was a significant interaction of variant type and time on pendrin abundance ($P<0.0001$), that is, the pendrin half-life differed depending on the individual variant. Specifically, pendrin protein variants p.L236P and p.R409H were degraded more rapidly compared with the wild-type (Fig. 1A and B). For each variant, data have been normalized for the corresponding expression levels at time 0 and therefore show expression level 1 at this time point (Fig. 1B), but absolute expression levels of p.L236P and p.R409H variants are indeed reduced compared with the wild-type (Fig. 1A, 0 h).

The transcript and protein expression of pendrin were also tested in a knock-in mouse model of Pendred syndrome/DFNB4 bearing the pendrin variant p.L236P. The mouse exhibits mild to profound hearing loss and vestibular dysfunction (20). The protein expression levels of p.L236P variant were significantly reduced in the kidneys of homozygous mutant mice compared with their wild-type littermates with no reduction in transcript levels, ruling out the possibility that the reduced pendrin protein abundance in p.L236P mice is due to reduced transcription or mRNA instability and indicating that an accelerated degradation of the pathogenic pendrin variant also occurs in native tissue (Fig. 1C). The ion transport function determined as iodide influx in transfected cells, the total protein abundance, and the plasma membrane protein abundance of wild-type pendrin and seven pendrin variants characterized in our previous study (26), as well as pendrin variants p.L236P and p.R409H, are shown in Fig. 1D-F. Total protein abundance (Fig. 1D), as well as plasma membrane protein abundance (Fig. 1E), correlated positively with ion transport function. These observations support the hypothesis that a reduction in protein function derives from a reduction

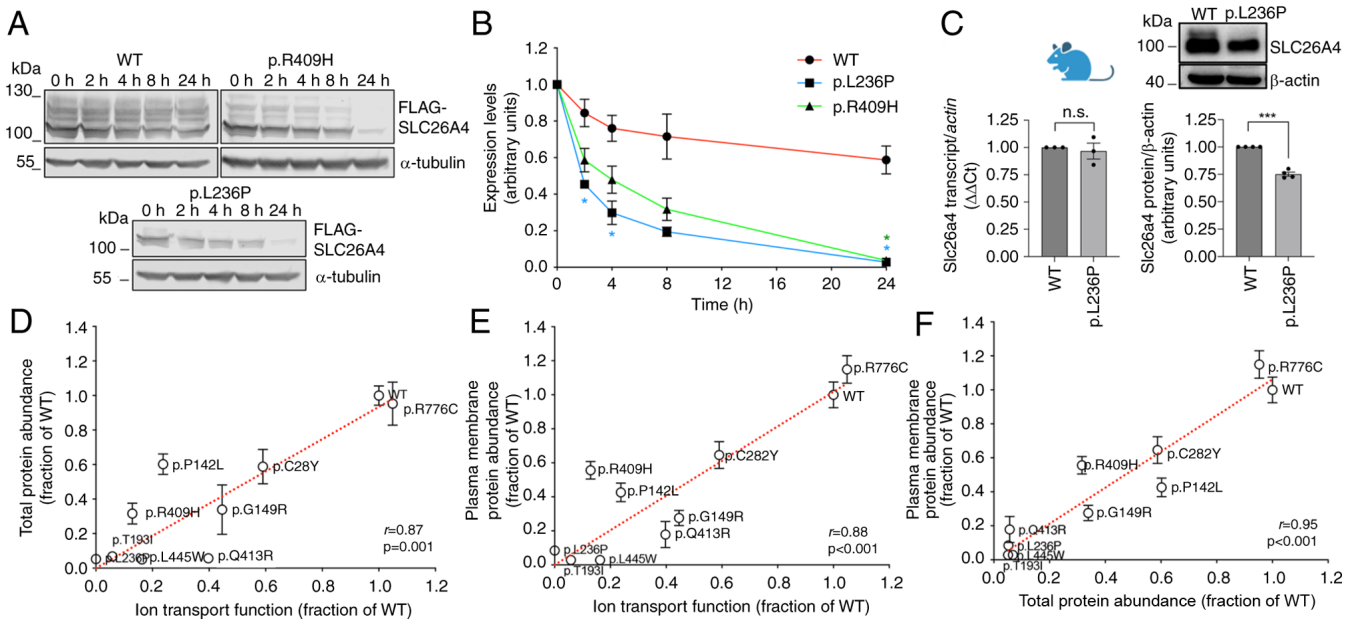

Figure 1. The protein half-life of pathogenic pendrin variants is significantly reduced compared with the wild-type, and reduced protein levels correlate to reduced function. (A) Original western blots and (B) half-life measurements of wild-type pendrin or pendrin variants p.L236P and p.R409H in 293 Phoenix cells transfected for 24 h with the pFLAG vector and incubated with 25 μg/ml cycloheximide for 0-24 h. *P<0.05, vs. wild-type, two-way ANOVA with Tukey's multiple comparison post-test. 3<n<4; n refers to the number of independent experiments. For each time point, data have been normalized for the expression levels of the respective variant at time 0. (C) Slc26a4 transcript levels (n=3) and original western blot and densitometry (n=4) of pendrin expression in the crude lysates of whole kidneys from SLC26A4 p.L236P mice and their wild-type littermates. n refers to the number of independent samples. ***P<0.001, one-sample Student's t-test. n.s., not significant. (D-F) Ion transport function (the iodide influx of each individual variant was subtracted for the endogenous iodide influx measured in control cells; 42<n<72 independent measurements from at least 3 independent experiments), total protein abundance (n=16 independent measurements from at least 3 independent experiments), and plasma membrane protein abundance (n=16 independent measurements from at least 3 independent experiments) of wild-type pendrin and seven pendrin variants [raw data received from de Moraes *et al* (26)] plus p.L236P and p.R409H (raw data taken from Figs. 4D, 3B and 4B respectively, white bars) were expressed as fraction of the wild-type and positive correlation between data sets was tested by linear regression. Pearson's r and two-tailed P-values are indicated.

in protein expression. Total protein abundance and plasma membrane protein abundance were also positively correlated (Fig. 1F). As the plasma membrane fraction is the functional form of the anion exchanger, these data indicate that increasing the total protein abundance might rescue plasma membrane protein abundance and, consequently, protein function.

Wild-type pendrin and its pathogenic variants are ubiquitinated. 293 Phoenix cells were transfected with N-terminally flagged wild-type pendrin and pendrin variants p.R409H and p.L236P and treated with a specific inhibitor of 26S proteasome (1 μM MG132 for 16 h) to induce the accumulation of ubiquitinated proteins. Pendrin was immunoprecipitated with an anti-FLAG antibody from whole-cell lysates and the immunoprecipitated proteins were probed with an anti-ubiquitin antibody. A clear band corresponding to the MW of pendrin denoted that wild-type pendrin and both variants are abundantly ubiquitinated (Fig. 2A and B). These results indicated that the reduction of expression of pathogenic pendrin variants may derive from their ubiquitination and consequent accelerated degradation via the UPS.

To confirm the ubiquitination of the pendrin protein and to experimentally identify sites of ubiquitination within the polypeptide, wild-type pendrin and pendrin variant p.R409H were immunoprecipitated from 293 Phoenix cells treated with MG132 or the vehicle and submitted to LC-MS/MS analysis (Fig. 2C). After trypsin enzymatic digestion, 29 peptides were produced for the wild-type and 28 for the p.R409H variant (Table SI). From the MS/MS analysis, 6 GlyGly-modified peptides were identified in the MG132-treated and vehicle-treated wild-type pendrin samples and 5 in the MG132-treated and vehicle-treated pendrin p.R409H samples. The lysine residue at position p.77 was found to be modified in the vehicle-treated wild-type samples, albeit with low intensity, reflecting a lower abundance of the corresponding modified peptide, and in the MG132-treated p.R409H samples at greater intensity. Lysine 329 was only modified in MG132-treated p.R409H samples. Lysine at position 537 was found modified in both MG132-treated and vehicle-treated wild-type samples and the MG132-treated p.R409H samples. Lysine 546 was found modified in all samples but with lower intensity in the vehicle-treated p.R409H samples. Lysine 563 and 564 were found to be modified only in the wild-type samples. Lysine 681 was found modified in the vehicle-treated wild-type samples and the MG132-treated p.R409H samples (Fig. 2C and D).

To verify which of these ubiquitination sites control pendrin degradation, sequential C-terminal SLC26A4 truncations were designed (Fig. 2D), and the stability of the corresponding polypeptides was verified by western blotting (Fig. 2E and F). Expression of these constructs in cells gives rise to glycosylated polypeptides (Fig. S1A, left panel), as confirmed by deglycosylation of protein lysates prior to western blotting (Fig. S1A, right panel). As expected for pendrin variants, deletion of the C-terminus of pendrin leads to accelerated degradation of the p.738X, p.674X and p.584X protein products, as reflected by a reduction of protein abundance compared with full-length

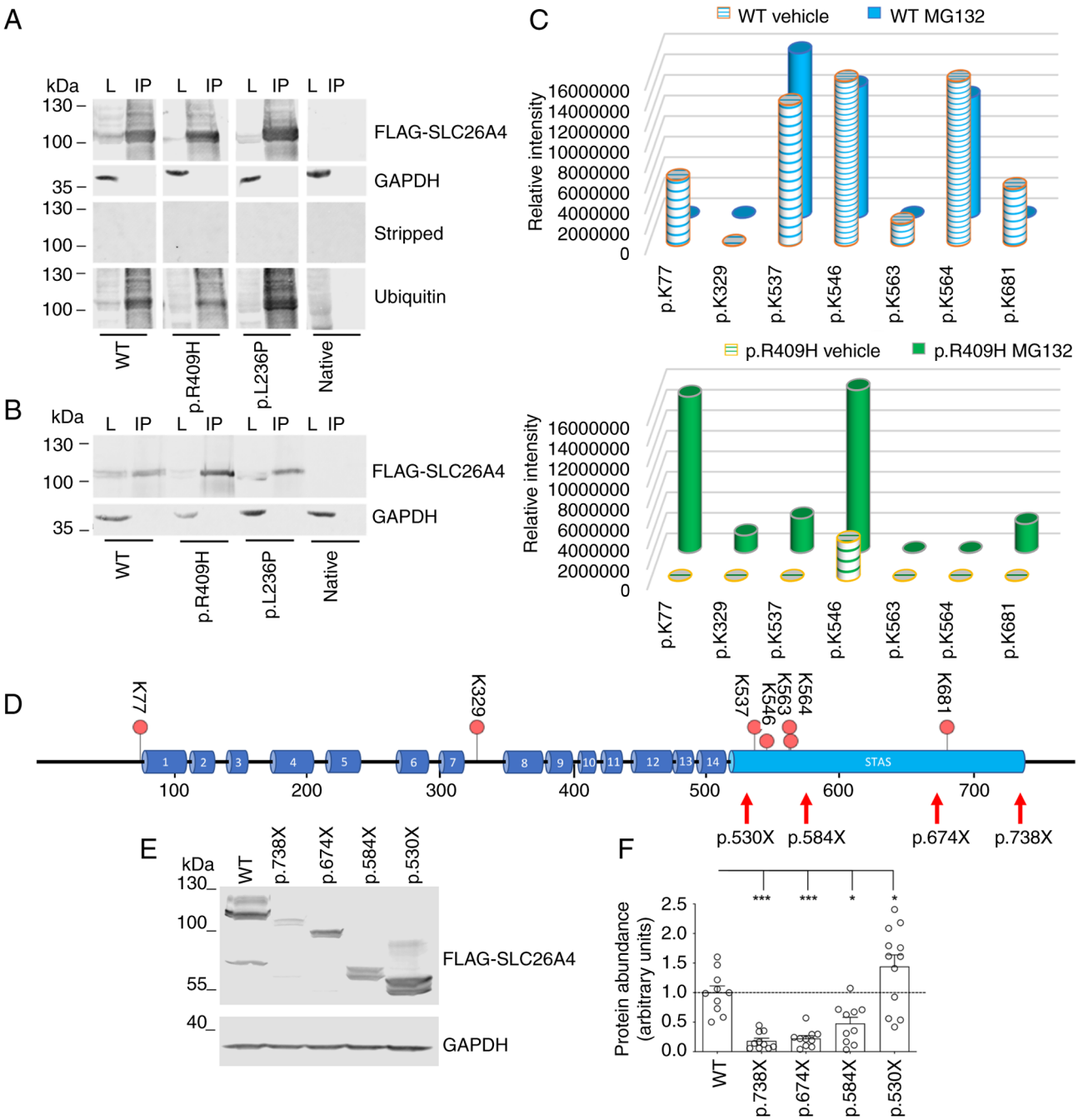

Figure 2. Wild-type pendrin and pathogenic pendrin variants are ubiquitinated. 293 Phoenix cells were transfected for 48 h with plasmid vectors encoding N-terminally FLAG-tagged wild-type pendrin or pendrin variants p.R409H and p.L236P (pFLAG vector) and incubated with the proteasome inhibitor MG132 (1 μM) for 16 h. (A) Pendrin was immunoprecipitated from whole cell lysates with an anti-FLAG antibody. The immunoprecipitated proteins were subjected to western blot analysis with anti-FLAG and anti-GAPDH antibodies. Then, membranes were stripped and probed with an anti-ubiquitin antibody. The image is representative of 3 independent experiments. (B) In an independent experiment, the immunoprecipitated proteins were submitted to deglycosylation before western blotting. The smear in the IP lanes in A was absent in B and therefore corresponds to glycosylated pendrin. (C) Intensity of the signal of each GlyGly-modified lysine identified by MS analysis in samples immunoprecipitated from wild-type pendrin and pendrin p.R409H transfected cells, respectively; a stronger signal corresponds to a higher abundance of ubiquitin-modified lysine residues at each specific position. (D) Graphic representation of the pendrin full-length polypeptide. The blue and turquoise cylinders indicate the approximate amino acid position of the 14 transmembrane segments and the STAS domain, respectively, according to Wang *et al* (52) for *Sus scrofa* pendrin. The red circles above the sequence correspond to all lysines found to be ubiquitinated in the LC-MS/MS analysis. The red arrows indicate sequential C-terminal truncations designed for the experiments shown in E-F. (E) Original western blot, and (F) densitometry of whole cell lysates from cells transfected with N-terminally FLAG-tagged wild-type full-length pendrin or the indicated C-terminal truncations (pFLAG vector). The densitometry considered both the unglycosylated and the glycosylated proteins. 10<n<12 independent experiments. ***P<0.001 and *P<0.05 vs. wild-type, one-way ANOVA with Dunnet's post-hoc test.

pendrin (Fig. 2F). However, removal of the four ubiquitination sites Lys537, Lys546, Lys563 and Lys564 led to stabilization of the p.530X fragment compared with full-length pendrin and the p.738X, p.674X and p.584X fragments, denoting that these ubiquitination sites play an important role in the degradation of wild-type pendrin (Fig. 2F).

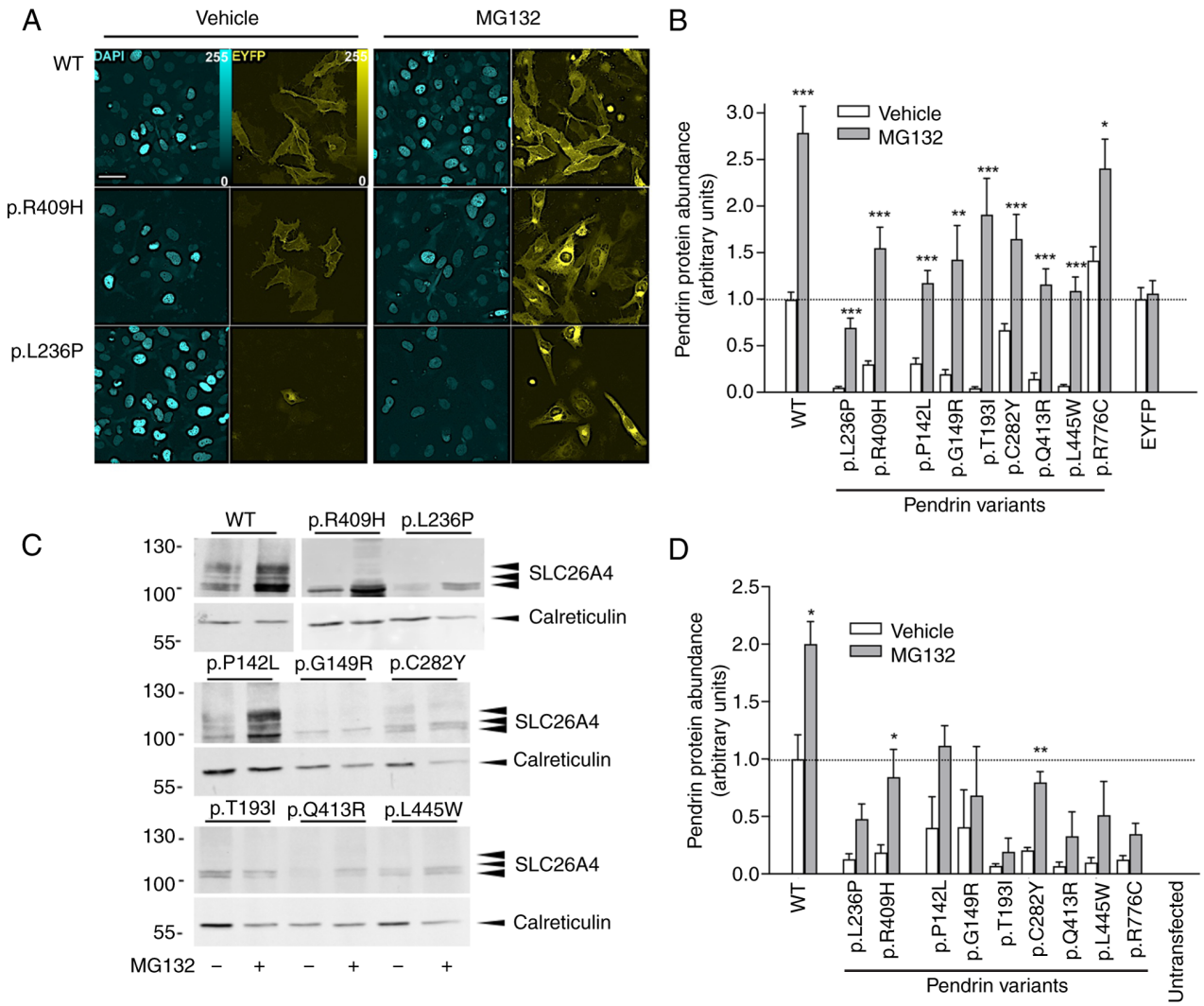

Figure 3. Inhibition of UPS increases total protein levels of wild-type pendrin and its variants. (A) HeLa cells were transfected for 72 h with plasmid vectors encoding wild-type or mutant SLC26A4-EYFP (pEYFPN1 vector) and incubated with the proteasome inhibitor MG132 (10 μM) or the vehicle (0.1% DMSO) for 16 h. Scale bar, 50 μm. (B) Total expression levels of pendrin variants were determined by quantitative imaging and normalized for those of the wild-type. ***P<0.001, **P<0.01 and *P<0.05 vs. vehicle; two-tailed, unpaired Student's t-test. 8<n<18 from 3 independent experiments. n corresponds to the number of whole imaging fields. (C) Representative images, and (D) densitometry of western blots on total cellular membranes from 293 Phoenix cells transfected with wild-type or mutant SLC26A4 for 48 h (pTARGET vector) and incubated with MG132 (10 μM) or the vehicle (0.1% DMSO) for 16 h. **P<0.01 and *P<0.05 vs. vehicle, two-tailed, unpaired Student's t-test (n=3 independent experiments). The p.R776C variant was not recognized by the antibody as the amino acid substitution falls within the antibody epitope. WT, wild-type.

Exposure of cells to MG132 led to a significant increase in protein expression of full-length pendrin (109% increase) and p.738X (156% increase), p.674X (233% increase) and p.584X (497% increase) fragments, but only a modest increase (37%) of p.530X fragment, denoting that the amino acid sequence 530-584, containing Lys537, Lys546, Lys563 and Lys564, is essential for responsiveness to proteasome inhibitors and supporting the important role of these ubiquitination sites in pendrin degradation (Fig. S1B).

Wild-type pendrin and its pathogenic variants are degraded by the UPS. It was investigated whether ubiquitination and increased degradation by the UPS might explain the reduction in the expression of naturally occurring pathogenic pendrin variants. Pendrin variants were ectopically expressed, and their total protein abundance was measured using quantitative imaging (Fig. 3A and B). The expression of all variants, except for the fully functional variant p.R776C, was significantly reduced compared with the wild-type (one-way ANOVA with Dunnet's post-hoc test), which is in agreement with our previous findings (26). Exposure of cells to MG132 significantly increased the total protein levels of all variants tested. Expression of the transfection marker EYFP was unaffected. Testing of protein expression via western blotting on total cellular membranes led to similar results (Fig. 3C and D).

Inhibitors of the 26S proteasome rescue plasma membrane expression and function of pathogenic pendrin variants. Pendrin variants were ectopically expressed and their protein abundance in the plasma membrane region was measured by quantitative imaging in the presence and absence of MG132. The plasma membrane expression levels of all variants, except for the fully functional variant p.R776C, were significantly

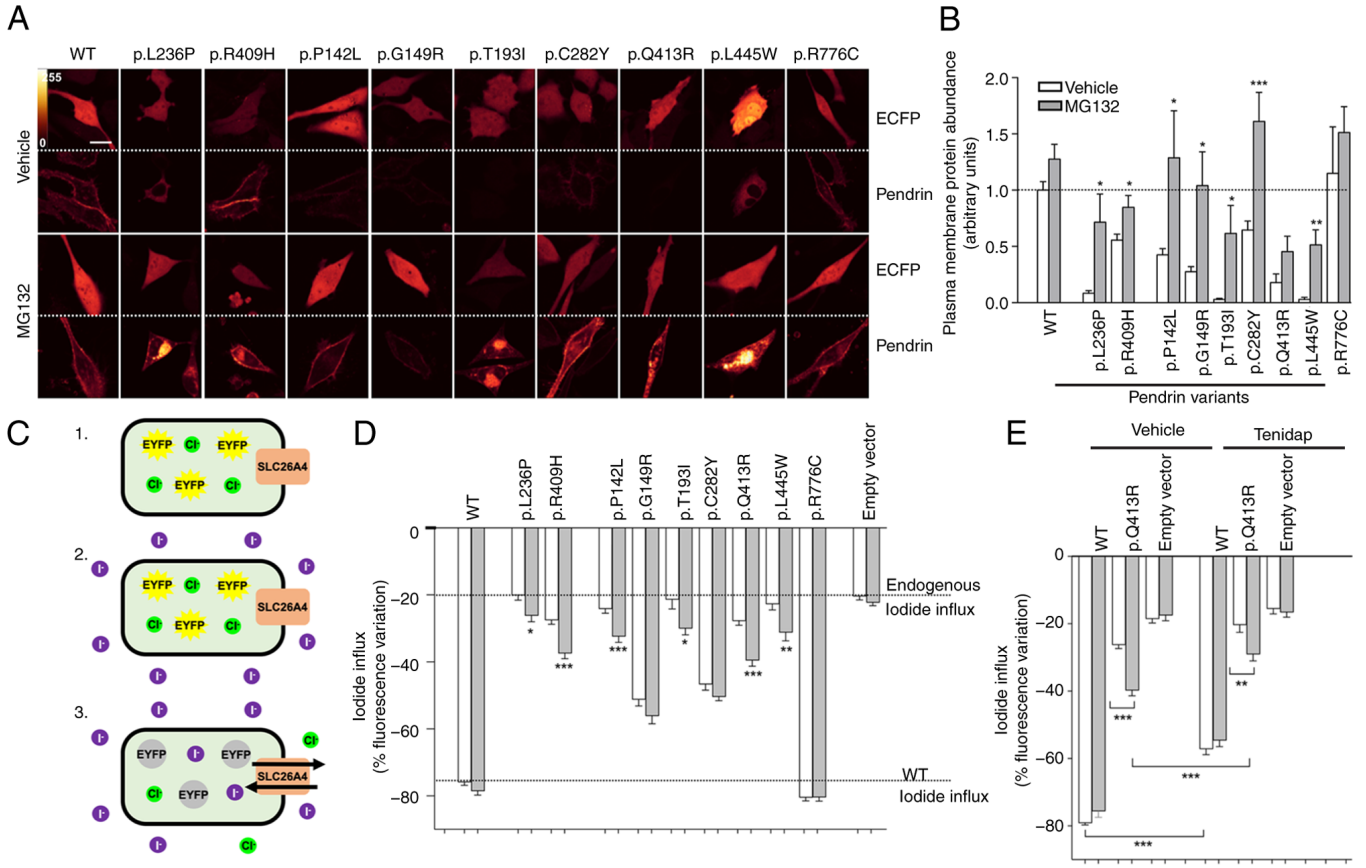

Figure 4. Inhibition of ubiquitin-proteasome system increases plasma membrane protein levels and function of pathogenic pendrin variants. (A) HeLa cells were transfected for 72 h with pEYFPN1 vectors encoding the wild-type or mutant SLC26A4-EYFP and the transfection marker ECFP and incubated with the proteasome inhibitor MG132 (10 μM) or the vehicle (0.1% DMSO) for 16 h. Scale bar, 25 μm. (B) Plasma membrane levels of pendrin variants were determined by quantitative imaging and normalized for those of the wild-type. ***P<0.001, **P<0.01 and *P<0.05 vs. vehicle, two-tailed, unpaired Student's t-test. 11<n<21 from 3 independent experiments. n corresponds to the number of cells. (C) Fluorometric method for evaluation of pendrin ion transport. Cells transfected with wild-type or mutant pendrin (pTARGET vector) and the iodide sensor EYFP H148Q:I152L for 48 h (1) are exposed to an iodide-rich extracellular solution (2). Iodide (magenta) enters the cell in exchange for chloride (green), determining the quenching of EYFP H148Q:I152L fluorescence (3). The % fluorescence decrease is a measure of ion transport efficiency. (D and E) 293 Phoenix cells were co-transfected for 48 h with the pTARGET vector encoding the wild-type or mutant pendrin or an empty vector and the iodide sensor EYFP H148Q:I152L and incubated with the proteasome inhibitor MG132 (10 μM) or the vehicle (0.1% DMSO) for 6 h. Ion transport activity was determined with the fluorometric method. ***P<0.001, **P<0.01 and *P<0.05 compared with vehicle, two-tailed, unpaired Student's t-test. (E) 100 μM tenidap or its vehicle (0.1% DMSO) were added to the experimental solutions. ***P<0.001 and **P<0.01, one-way ANOVA with Bonferroni's post-hoc test. Data are from at least 3 independent experiments with n=6 each. n corresponds to a well of a 96-well plate. WT, wild-type.

reduced compared with the wild-type (one-way ANOVA with Dunnet's post-hoc test), consistent with previous results (26). The plasma membrane protein expression significantly increased following treatment with MG132 for most variants, except the wild-type and the fully functional variant p.R776C (Fig. 4A and B).

The ion transport activity of all pendrin variants was measured as iodide influx in transfected cells via a fluorometric method in the presence and absence of MG132 (Fig. 4C). For this, cells were co-transfected with the pTARGET and pEYFPN1 p.H148Q;I152L vectors. The successful transfection of the pTARGET constructs into cells is documented by western blotting (Fig. 3C and D; white bars). The activity of all variants, except for the fully functional variant p.R776C, was significantly reduced compared with the wild-type (one-way ANOVA with Dunnet's post-hoc test), in agreement with our previous findings (26). Exposure of cells to MG132 led to a statistically significant rescue of ion transport activity in 75% (6/8) of the pathogenic variants tested. Specifically, the partially functional pathogenic variant p.R409H exhibited a ~113% recovery of ion transport function (n=30, P<0.001 vs. vehicle, Fig. 4D). The basal iodide influx measured in cells not expressing pendrin did not respond to MG132, indicating that the MG132-increased iodide influx is independent of endogenous ion transporters and/or channels.

It was previously reported that pendrin is resistant to the classical inhibitor of anion exchangers 4,4'-diisothiocyano-2, 2'-stilbene-disulfonic acid (DIDS) but is inhibited by the anti-inflammatory drug tenidap (41). Accordingly, the function of pendrin variant p.Q413R measured in the presence of MG132 was significantly inhibited by tenidap (Fig. 4E), further supporting the conclusion that the MG132-induced iodide influx is pendrin-dependent. Collectively, these findings indicated that the UPS regulates the expression levels of wild-type pendrin and leads to accelerated degradation of pathogenic pendrin variants, therefore causing their loss of function. Inhibition of UPS can lead to a partial recovery of the ion transport activity of some of the functionally impaired pendrin variants.

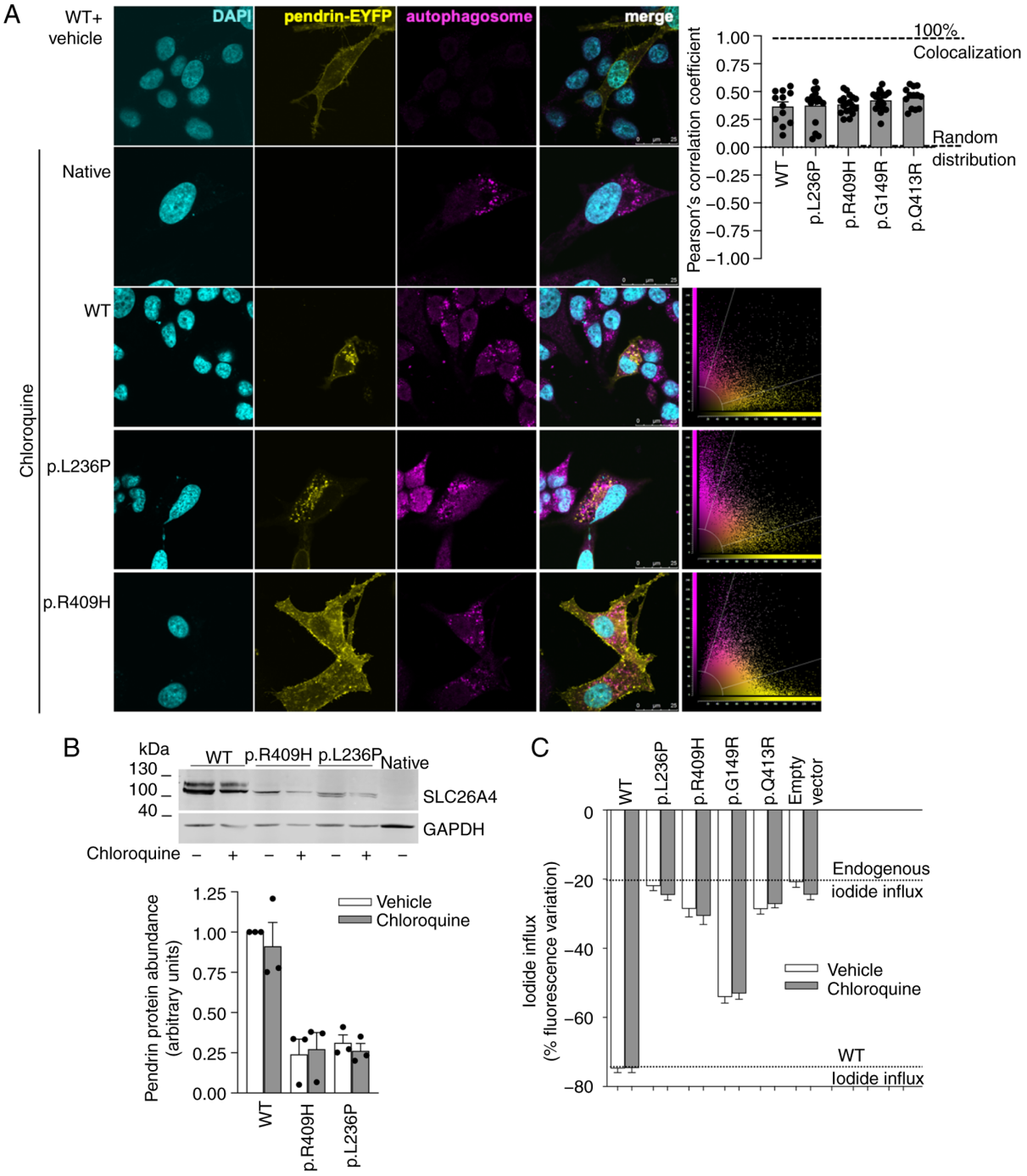

Figure 5. Inhibition of the lysosomal and autophagosomal pathways does not affect the localization and function of pathogenic pendrin variants. (A) HeLa cells were transfected for 72 h with pEYFPN1 vectors encoding the wild-type or mutant SLC26A4-EYFP and incubated with chloroquine (200 μM) or the vehicle (water) for 16 h. Scale bar, 25 μm. Colocalization with the autophagosome was determined by confocal imaging and represented with Pearson's correlation coefficient. No statistically significant differences compared with wild-type were found, one-way ANOVA with Dunnet's post-hoc test, 12<n<18 from 3 independent experiments. n corresponds to the number of cells. (B) Representative blot (top), and densitometry (bottom) of western blots on total cellular proteins from 293 Phoenix cells transfected with the pFLAG vector coding wild-type or mutant SLC26A4 for 48 h and incubated with chloroquine (200 μM) or the vehicle (water) for 6 h. No statistically significant differences between pendrin expression levels in the presence of chloroquine and its vehicle were found (two-tailed, unpaired Student's t-test). n=3 independent experiments. (C) 293 Phoenix cells were co-transfected for 48 h with pTARGET vectors encoding the wild-type or mutant pendrin and the iodide sensor EYFP H148Q:I152L and incubated with chloroquine (200 μM) or the vehicle (water) for 16 h. Ion transport activity was determined with a fluorometric method. No statistically significant differences between pendrin activity in the presence of chloroquine and its vehicle were found (two-tailed, unpaired Student's t-test). Data are from at least 3 independent experiments with n=6 each. n corresponds to a well of a 96-well plate. WT, wild-type.

The autophagosomal and lysosomal degradation pathways are not involved in the regulation of wild-type pendrin and pendrin variants. It was tested whether the autophagosomal and lysosomal pathways might be responsible for pendrin degradation. Pendrin variants were ectopically expressed and the accumulation of autophagosomes was induced following exposure of cells to chloroquine. Chloroquine mainly inhibits the autophagic flux by impairing the fusion of autophagosomes

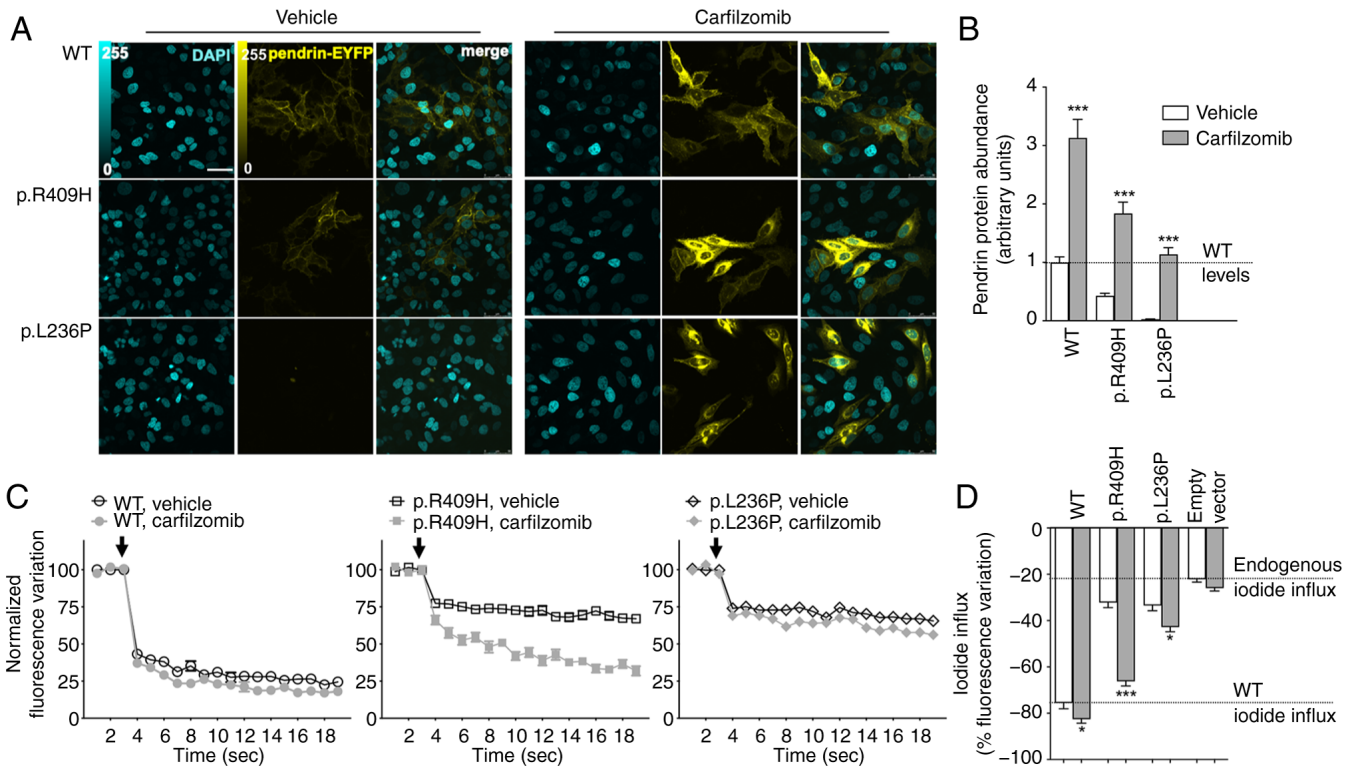

Figure 6. Inhibition of ubiquitin-proteasome system with carfilzomib rescues expression and function of pathogenic pendrin variants. (A) HeLa cells were transfected for 72 h with pEYFPN1 vectors encoding the wild-type or mutant SLC26A4-EYFP and incubated with carfilzomib (1 μM) or the vehicle (0.01% DMSO) for 16 h. Scale bar, 50 μm. (B) Total expression levels of pendrin variants were determined by quantitative imaging and normalized for those of the wild-type. ***P<0.001 compared with vehicle (two-tailed, unpaired Student's t-test). n=18 from 3 independent experiments with n=6 each. n corresponds to whole imaging fields. (C) 293 Phoenix cells were co-transfected for 48 h with pTARGET vectors encoding the wild-type or mutant pendrin or an empty vector and the iodide sensor EYFP H148Q:I152L and incubated with carfilzomib (10 μM) or the vehicle (0.1% DMSO) for 16 h. Ion transport activity was determined with the fluorometric method by measuring intracellular fluorescence over time before and after the addition of iodide to the extracellular solution (arrows). (D) Iodide influx expressed as the % decrease of the intracellular fluorescence. ***P<0.001 and *P<0.05 compared with vehicle (two-tailed, unpaired Student's t-test). n=24 from 4 independent experiments with n=6 each. n corresponds to a well of a 96-well plate. WT, wild-type.

with lysosomes (45). The possible presence of pendrin and its variants within autophagosomes was verified by co-localization with an autophagosomal marker. Results show a lack of preferential localization of wild-type pendrin or pendrin variants within autophagosomes (Fig. 5A). In addition, chloroquine failed to increase the expression levels of pendrin variants p.L236P and p.R409H (Fig. 5B) and did not rescue the function of four pendrin variants, three of which were responsive to MG132 (Fig. 5C). These findings denoted that the autophagosomal and lysosomal degradation pathways are likely not involved in the regulation of the expression levels of pendrin and its variants and can unlikely be targeted to rescue their expression and/or function.

Clinically approved UPS inhibitors rescue plasma membrane expression and function of pathogenic pendrin variants. The FDA/EMA-approved proteasome inhibitors bortezomib and carfilzomib and the investigational proteasome inhibitor delanzomib were tested on wild-type, p.L236P and p.R409H pendrin expression and function. Exposure of cells to 1 μM bortezomib, carfilzomib, or delanzomib for 16 h significantly increased the total protein abundance of wild-type pendrin and both variants (Fig. S2). These proteasome inhibitors (1-10 μM for 6-16 h) were also tested on pendrin function, and a significant rescuing effect was observed in most conditions (Figs. S3-S5). Again, the partially functional variant p.R409H proved to be particularly responsive to proteasome inhibition, and its activity was rescued to levels close to those of the wild-type (60% of vehicle-treated wild-type activity subtracted for the proteasome-treated endogenous iodide influx with 1 μM bortezomib for 16 h; 75% with 10 μM carfilzomib for 16 h; and 61% with 10 μM delanzomib for 16 h). Concerning variant p.L236P, the best rescuing effect (31.5% of wild-type activity) was obtained with 10 μM carfilzomib for 16 h. Although the expression of the wild-type was increased following exposure to proteasome inhibitors (Fig. S2), the wild-type function and the endogenous iodide transport were mostly unaffected (Figs. S3-S5). Data of carfilzomib are summarized in Fig. 6. Although cell viability was reduced following incubation with the proteasome inhibitors according to the cell proliferation test (Fig. S6A-D), the number of cells was not reduced (Fig. S6E), indicating that the cell proliferation test revealed a metabolic slowdown rather than cell death, which would have caused cell loss.

Lumacaftor, tezacaftor, elexacaftor, rapamycin, and ataluren failed to rescue the function of pathogenic pendrin variants. Lumacaftor (VX-809) is a pharmaceutical chaperone referred to as a cystic fibrosis transmembrane conductance regulator (CFTR) corrector acting on the ER. It allows a fraction of ΔF508 CFTR to adopt a properly folded form and mobilize from the ER to the cell surface for normal functioning (46).

Tezacaftor (VX-661) and elexacaftor (VX-445) also act as CFTR correctors and are used in combination with ivacaftor, which is a potentiator that increases the ion channel function (47). Ataluren is a potent non-sense-suppressing agent that selectively induces ribosomal read-through of premature but not normal termination codons and was proposed for class I mutations in cystic fibrosis (48). Concentrations of lumacaftor, tezacaftor, and elexacaftor well above their EC50 failed to rescue the function of pendrin p.L236P and p.R409H variants in our experimental setting. Ataluren was ineffective in increasing the function of pendrin p.335X (Fig. S7).

Rapamycin is an mTOR inhibitor and was shown to relieve cell death of patient-derived iPSC cells (49). Rapamycin failed to rescue the function of pendrin p.L236P and p.R409H variants in our experimental setting (Fig. S7).

Discussion

Several studies tested pathogenic pendrin variants in heterologous expression systems and showed that only ~50% of these variants remain trapped within the ER and manifest a severe loss of function. In contrast, other pathogenic variants are correctly localized at the plasma membrane and have a significant residual function (26,27,36,37,39,40,42,50). It has been previously shown that the total protein abundance and plasma membrane protein levels of pathogenic pendrin variants were significantly reduced compared with the wild-type when ectopically expressed, regardless of their subcellular localization. Reduction in protein levels was not associated with an alteration in the corresponding mRNA levels (26,27). Half-life measurements showed that decreased protein expression derives from accelerated protein degradation of the pathogenic variants rather than decreased protein production or cell loss (Fig. 1A and B). The protein expression of the common variant p.L236P was reduced compared with that of the wild-type in the kidneys of a knock-in mouse (20). A reduction in transcript levels was not observed, leading to the exclusion of defective transcription or mRNA instability as causative factors in this context (Fig. 1C). Thus, the reduction in protein levels, rather than ER trapping, constitutes the main pathological mechanism of Pendred syndrome/DFNB4.

MS analysis confirmed the ubiquitination of wild-type pendrin and showed the ubiquitination of pendrin variants p.L236P and p.R409H, with multiple modification sites being identified (Fig. 2A-C). A total of 4 identical ubiquitination sites (p.K77, p.K537, p.K546 and p.K681) were found in the wild-type as well as the p.R409H variant, while p.K563 and p.K564 were only ubiquitinated in the wild-type and p.K329 only in the p.R409H samples. Interestingly, the lysines at positions 77, 329, 546 and 681 were also predicted as highly probable ubiquitination sites by the online tool RUBI (51), with a probability score of 0.5112, 0.2972, 0.3236 and 0.3627, respectively. Assessing the stability of pendrin following sequential deletions of the C-terminus (Fig. 2D; the pendrin structure is represented according to (52) allowed for determining which of these ubiquitination sites controls the turnover of the wild-type variant. Removal of the C-terminus of pendrin (p.738X) greatly destabilizes the protein, and removal of Lys681 (p.674X construct) does not improve protein stability, the marginal role of Lys681 being also confirmed by its scarce ubiquitination levels. By contrast, removing the four ubiquitination sites between Lys537 and Lys564 (p.530X construct) leads to the stabilization of the polypeptide (Fig. 2E and F) and greatly reduces responsiveness to proteasome inhibition (Fig. S1B), pointing to a fundamental role of these residues in the degradation of wild-type pendrin.

For the wild-type samples, the ubiquitination profile is similar before and after inhibition of UPS with MG132, which did not increase the ubiquitination abundance. Interestingly, the p.R409H variant showed a different pattern, with very scarce ubiquitination levels and only one site being modified (p.K546) in the untreated samples and five ubiquitinated lysine residues, including p.K546, being detected upon treatment with MG132. Two of these sites (p.K77 and p.K546) showed particularly high ubiquitination levels, and one of these (p.K77) was not detected in the MG132-treated wild-type samples. This points to an important role of p.K77 in the degradation of the p.R409H variant.

MG132 treatment allows for the accumulation of those protein species that would otherwise undergo rapid proteasomal degradation. The low level of modified lysine residues in the vehicle-treated p.R409H samples is consistent with the prompt degradation of this pendrin variant by the UPS, whereas blocking the proteasome with MG132 allows for ubiquitinated proteins to accumulate in the cell, which permits their detection. Conversely, the wild-type form is more stable than the variant, and the ubiquitinated protein can be detected even in the absence of proteasomal inhibition. This is consistent with the half-life measurements showing a relatively longer half-life of the wild-type polypeptide and rapid degradation of the p.R409H variant (Fig. 1A and B).

Membrane transporters and channels are large and complex amphipathic multi-domain proteins, and their folding process may be slow and inefficient. Therefore, the same pathway may be involved in the degradation of the wild-type and mutant proteins. The folding of both the wild-type and the cystic fibrosis-associated mutant ΔF508 CFTR is inefficient, and mutant proteins are degraded by a process that is kinetically and pharmacologically indistinguishable from the process involved in the degradation of the misfolded immature wild-type CFTR (53). Additional examples of wild-type and pathogenic variants targeted to proteasomal degradation by the same mechanism include the ClC1 channels (54), Kv10.1 K^+ channels (55) and long QT syndrome 2 HERG channels (56). As wild-type pendrin is a slow-folding protein (28), it is unsurprising that the UPS can control the expression levels of both the wild-type protein and its pathogenic variants. However, differential ubiquitination to a specific site might lead to preferential degradation of the pathogenic variants. Comparing the wild-type and p.R409H variant ubiquitination profile upon UPS inhibition, it appears that ubiquitination of lysine residue p.K546 might participate in the degradation of both the wild-type and p.R409H variant, while lysine residue p.K77 can be responsible for the preferential degradation of p.R409H variant, and possibly other pendrin variants (Fig. 2C).

It was tested whether UPS inhibition might rescue the protein levels of pendrin and its variants. Inhibition of UPS with MG132 effectively increased the total protein levels of all pendrin variants tested, including the wild-type and a benign variant (Fig. 3). These data show that, following ubiquitination,

wild-type pendrin and its variants undergo UPS-mediated protein degradation, with minor involvement of the lysosomal/autophagosomal pathway (Fig. 5) and provide proof of concept that pharmacological inhibition of UPS rescues their expression.

As total protein abundance, plasma membrane protein abundance and ion transport function are positively correlated (Fig. 1D-F), it was postulated that increasing total protein abundance should increase plasma membrane protein abundance and, hence, ion transport function. As expected, the increase in pendrin total protein level following UPS inhibition (Fig. 3) was paralleled by a significant increase in protein levels of pathogenic variants in the plasma membrane (Fig. 4A and B) and led to a modest, although significant, increase in function for most of these variants (Fig. 4D). This indicates that misfolded pendrin variants might conserve at least in part their ion transport ability. However, the different variants variably responded to MG132, and the increase in expression did not always lead to a significant increase in function. The ion transport function of variants p.G149R and p.C282Y did not respond to MG132 (Fig. 4D) despite the significant increase in their plasma membrane levels (Fig. 4B). By contrast, the function of variants p.R409H and p.Q413R showed a 112 and 135% increase in the presence of MG132, respectively (the iodide influx of each variant was corrected for the endogenous iodide influx measured in cells transfected with the empty vector, $P<0.001$, unpaired, two-tailed Student's t-test; Fig. 4D). The reason for this inhomogeneous behavior amongst variants is currently unclear and might reflect biophysical properties of each individual variant, such as alterations in affinity for the transported ion(s) and/or interference with the conformational changes necessary to ion transport, that are not rescued by an increase in protein levels. Thus, although all tested variants responded to proteasomal inhibition concerning their expression levels, it cannot be assumed that an increase in protein abundance will increase the function of all pathogenic pendrin variants. Systematic functional testing of variants will be required to identify or predict those responding to proteasomal inhibition.

It also has to be noted that some variants deviate from the linear relationship between protein levels and function. For example, p.Q413R variant exhibits significant function (40% of the wild-type) despite almost undetectable protein levels (Fig. 1D). It is tempting to hypothesize that the amino acid substitution of glutamine (uncharged and polar) to arginine (positively charged at physiological pH) may lead to protein misfolding, degradation and reduced cellular abundance while simultaneously conferring an increased affinity for the transported ions, thereby increasing the transport efficiency (26). Accordingly, the function of this variant responded well to the inhibition of proteasomal degradation (Fig. 4D) despite a modest increase in protein levels in the plasma membrane (Fig. 4B).

Variants p.R409H and p.L236P were selected for further studies in that they are relatively common in the Caucasian population and are representative of pendrin variants that remain trapped in the ER with minimal residual function (p.L236P) and variants with correct targeting to the plasma membrane with significant residual function (p.R409H). Inhibition of UPS with bortezomib, carfilzomib and delanzomib effectively increased protein levels and ion transport function of pendrin p.R409H and p.L236P (Figs. 6 and S2-S5). Carfilzomib, which irreversibly inhibits the chymotrypsin-like activity of the 20S proteasome via a covalent bond, gave the best results and rescued the function of pendrin p.R409H to wild-type levels (Fig. 6). These findings indicate that, among pendrin variants, those targeting the plasma membrane and conserving residual function can represent candidates for molecular rescue.

Bortezomib, delanzomib and carfilzomib are in clinical use or being tested in clinical trials for the treatment of some forms of cancer including multiple myeloma (57) and, among these, bortezomib is a favorable candidate for drug repositioning in kidney fibrosis and systemic lupus erythematosus (58,59). At the concentration and incubation time tested, the toxicity of these compounds was mostly due to a decrease in cell metabolic activity rather than cell death in our experimental setting (Fig. S6).

While UPS was initially considered to act as an unspecific degradation mechanism of misfolded proteins, it is now widely recognized as a regulatory pathway involved in the fine-tuning of the cellular abundance and, hence, control of the activity of specific targets by selective enzymatic reactions and discriminatory receptors (60). The mechanism of degradation by UPS requires polyubiquitination of the target protein via the sequential activity of E1 (ubiquitin-activating), E2 (ubiquitin-conjugating) and E3 (ubiquitin ligases) enzymes (61). Skp1, Cullins, F-box (SCF)-type E3 ligases act in a macromolecular complex that includes Cullins 1-7 and various classes of adaptor and receptor proteins to recruit a specific target for poly-ubiquitination and proteasomal degradation (62,63), thereby offering numerous opportunities for pharmacological intervention and drug development (61,64,65). Multiple plasma membrane ion and water transport proteins, including the chloride channel CFTR, the large conductance Ca^{2+} and voltage-activated K^+ (BK) channels, as well as ClC1 chloride channels, are regulated by the UPS (66,67,54).

The precise understanding of the mechanism leading to the degradation of pathogenic variants of proteins has proved to be crucial for the identification of novel drug targets and mechanistic therapeutic strategies. Studies on the misfolding and subsequent proteasomal degradation of CFTR led to the development of novel drugs for the treatment of cystic fibrosis, including lumacaftor/ivacaftor and triple therapy with the next-generation corrector elexacaftor plus tezacaftor and ivacaftor (46,47,68). Genetic ablation and pharmacological inhibition of the E3 ligase Rma1 (RNF5) ameliorated the pathological phenotype in a mouse model of cystic fibrosis and rescued the activity of ΔF508 CFTR in primary bronchial epithelial cells derived from patients (69,70). These studies underscore that the different molecular players of the UPS may represent promising drug targets. Further studies are needed to elucidate the composition of the molecular complex leading to the recruitment of pendrin to proteasomal degradation.

To conclude, these findings show that i) the cellular levels of wild-type pendrin are regulated by the UPS following ubiquitination of Lys residues between amino acid positions 537 and 564; ii) pathogenic pendrin variants undergo accelerated degradation via the UPS following abundant and preferential ubiquitination of Lys77, which reduces expression levels and leads to loss of function; iii) UPS inhibitors can

rescue expression of pathogenic pendrin variants at the cell surface and ion transport function. Although inhibitors of the end-activity of the proteasome can unlikely be used in the clinical setting of hearing loss, these experiments suggest that targeting specific molecular players within the degradation pathway of pendrin might represent a novel concept for the treatment of Pendred syndrome/DFNB4, at least concerning the common p.R409H variant and some selected variants.

Acknowledgements

The authors acknowledge Mrs Elisabeth Mooslechner, Institute of Pharmacology and Toxicology, Paracelsus Medical University, Salzburg, Austria, for her expert secretarial assistance.

Funding

The present study was supported in part by the Research and Innovation Fund of Paracelsus Medical University (grant nos. 2022-Iif-004-DOSSENA and FIZ RM&NT Talent Pool Senior Researcher 042023).

Availability of data and materials

The data generated in the present study may be requested from the corresponding author.

Authors' contributions

EB and SD conceptualized the study, curated data and developed methodology. EB, RJ, AM, FH, HN, SK, HZ, JG and SD conducted formal analysis, investigation and visualization, and wrote, reviewed and edited the manuscript. SD prepared the original of the manuscript and acquired funding. EB and SD confirm the authenticity of all the raw data.

Ethics approval and consent to participate

The present study was approved (approval no. SYDWLL-2021-76) by the Ethics Committee of the School of Life Science, Shandong University (Jinan, China).

Patient consent for publication

Not applicable.

Competing interests

The authors declare that they have no competing interests.

References

1. Everett LA, Morsli H, Wu DK and Green ED: Expression pattern of the mouse ortholog of the Pendred's syndrome gene (Pds) suggests a key role for pendrin in the inner ear. Proc Natl Acad Sci USA 96: 9727-9732, 1999.
2. Royaux IE, Wall SM, Karniski LP, Everett LA, Suzuki K, Knepper MA and Green ED: Pendrin, encoded by the Pendred syndrome gene, resides in the apical region of renal intercalated cells and mediates bicarbonate secretion. Proc Natl Acad Sci USA 98: 4221-4226, 2001.
3. Royaux IE, Suzuki K, Mori A, Katoh R, Everett LA, Kohn LD and Green ED: Pendrin, the protein encoded by the Pendred syndrome gene (PDS), is an apical porter of iodide in the thyroid and is regulated by thyroglobulin in FRTL-5 cells. Endocrinology 141: 839-845, 2000.
4. Dossena S and Paulmichl M: The role of Pendrin in health and disease. Springer International Publishing, Switzerland, 2017.
5. Honda K, Kim SH, Kelly MC, Burns JC, Constance L, Li X, Zhou F, Hoa M, Kelley MW, Wangemann P, *et al*: Molecular architecture underlying fluid absorption by the developing inner ear. Elife 6: e26851, 2017.
6. Kim HM and Wangemann P: Epithelial cell stretching and luminal acidification lead to a retarded development of stria vascularis and deafness in mice lacking pendrin. PLoS One 6: e17949, 2011.
7. Wangemann P, Itza EM, Albrecht B, Wu T, Jabba SV, Maganti RJ, Lee JH, Everett LA, Wall SM, Royaux IE, *et al*: Loss of KCNJ10 protein expression abolishes endocochlear potential and causes deafness in Pendred syndrome mouse model. BMC Med 2: 30, 2004.
8. Fugazzola L, Cerutti N, Mannavola D, Vannucchi G and Beck-Peccoz P: The role of pendrin in iodide regulation. Exp Clin Endocrinol Diabetes 109: 18-22, 2001.
9. Soleimani M: The multiple roles of pendrin in the kidney. Nephrol Dial Transplant 30: 1257-1266, 2015.
10. Brazier F, Corniere N, Picard N, Chambrey R and Eladari D: Pendrin: Linking acid base to blood pressure. Pflugers Arch 476: 533-543, 2024.
11. Wall SM: Regulation of blood pressure and salt balance by Pendrin-Positive intercalated cells: Donald seldin lecture 2020. Hypertension 79: 706-716, 2022.
12. Smith RJH: Pendred Syndrome/Nonsyndromic Enlarged Vestibular Aqueduct. In: GeneReviews®. Adam MP, Ardinger HH, Pagon RA, *et al* (eds), Seattle, WA, 1993.
13. Fraser GR: Association of congenital deafness with goitre (Pendred's Syndrome) a study of 207 families. Ann Hum Genet 28: 201-249, 1965.
14. Griffith AJ and Wangemann P: Hearing loss associated with enlargement of the vestibular aqueduct: Mechanistic insights from clinical phenotypes, genotypes, and mouse models. Hear Res 281: 11-17, 2011.
15. Choi BY, Kim HM, Ito T, Lee KY, Li X, Monahan K, Wen Y, Wilson E, Kurima K, Saunders TL, *et al*: Mouse model of enlarged vestibular aqueducts defines temporal requirement of Slc26a4 expression for hearing acquisition. J Clin Invest 121: 4516-4525, 2011.
16. Wangemann P: Mouse models for pendrin-associated loss of cochlear and vestibular function. Cell Physiol Biochem 32: 157-165, 2013.
17. Wangemann P and Griffith AJ: Mouse models reveal the role of pendrin in the inner ear. In: The role of pendrin in health and disease. Dossena S and Paulmichl M (eds). Springer International Publishing, Switzerland: 7-22, 2017.
18. Wangemann P, Nakaya K, Wu T, Maganti RJ, Itza EM, Sanneman JD, Harbidge DG, Billings S and Marcus DC: Loss of cochlear HCO3-secretion causes deafness via endolymphatic acidification and inhibition of Ca2+ reabsorption in a Pendred syndrome mouse model. Am J Physiol Renal Physiol 292: F1345-F1353, 2007.
19. Nishio A, Ito T, Cheng H, Fitzgerald TS, Wangemann P and Griffith AJ: Slc26a4 expression prevents fluctuation of hearing in a mouse model of large vestibular aqueduct syndrome. Neuroscience 329: 74-82, 2016.
20. Wen Z, Zhu H, Li Z, Zhang S, Zhang A, Zhang T, Fu X, Sun D, Zhang J and Gao J: A knock-in mouse model of Pendred syndrome with Slc26a4 L236P mutation. Biochem Biophys Res Commun 515: 359-365, 2019.
21. Taylor JP, Metcalfe RA, Watson PF, Weetman AP and Trembath RC: Mutations of the PDS gene, encoding pendrin, are associated with protein mislocalization and loss of iodide efflux: Implications for thyroid dysfunction in Pendred syndrome. J Clin Endocrinol Metab 87: 1778-1784, 2002.
22. Rotman-Pikielny P, Hirschberg K, Maruvada P, Suzuki K, Royaux IE, Green ED, Kohn LD, Lippincott-Schwartz J and Yen PM: Retention of pendrin in the endoplasmic reticulum is a major mechanism for Pendred syndrome. Hum Mol Genet 11: 2625-2633, 2002.
23. Dai P, Stewart AK, Chebib F, Hsu A, Rozenfeld J, Huang D, Kang D, Lip V, Fang H, Shao H, *et al*: Distinct and novel SLC26A4/Pendrin mutations in Chinese and U.S. patients with nonsyndromic hearing loss. Physiol Genomics 38: 281-290, 2009.

24. Choi BY, Stewart AK, Madeo AC, Pryor SP, Lenhard S, Kittles R, Eisenman D, Kim HJ, Niparko J, Thomsen J, *et al*: Hypo-functional SLC26A4 variants associated with nonsyndromic hearing loss and enlargement of the vestibular aqueduct: Genotype-phenotype correlation or coincidental polymorphisms? Hum Mutat 30: 599-608, 2009.
25. Wasano K, Takahashi S, Rosenberg SK, Kojima T, Mutai H, Matsunaga T, Ogawa K and Homma K: Systematic quantification of the anion transport function of pendrin (SLC26A4) and its disease-associated variants. Hum Mutat 41: 316-331, 2020.
26. de Moraes VCS, Bernardinelli E, Zocal N, Fernandez JA, Nofziger C, Castilho AM, Sartorato EL, Paulmichl M and Dossena S: Reduction of cellular expression levels is a common feature of functionally affected pendrin (SLC26A4) protein variants. Mol Med 22: 41-53, 2016.
27. Roesch S, Bernardinelli E, Nofziger C, Tóth M, Patsch W, Rasp G, Paulmichl M and Dossena S: Functional testing of SLC26A4 Variants-clinical and molecular analysis of a cohort with enlarged vestibular aqueduct from Austria. Int J Mol Sci 19: 209, 2018.
28. Shepshelovich J, Goldstein-Magal L, Globerson A, Yen PM, Rotman-Pikielny P and Hirschberg K: Protein synthesis inhibitors and the chemical chaperone TMAO reverse endoplasmic reticulum perturbation induced by overexpression of the iodide transporter pendrin. J Cell Sci 118: 1577-1586, 2005.
29. Lee K, Hong TJ and Hahn JS: Roles of 17-AAG-induced molecular chaperones and Rma1 E3 ubiquitin ligase in folding and degradation of Pendrin. FEBS Lett 586: 2535-2541, 2012.
30. Jung J, Kim J, Roh SH, Jun I, Sampson RD, Gee HY, Choi JY and Lee MG: The HSP70 co-chaperone DNAJC14 targets misfolded pendrin for unconventional protein secretion. Nat Commun 7: 11386, 2016.
31. Nanami M, Pham TD, Kim YH, Yang B, Sutliff RL, Staub O, Klein JD, Lopez-Cayuqueo KI, Chambrey R, Park AY, *et al*: The role of intercalated cell Nedd4-2 in BP regulation, Ion transport, and transporter expression. J Am Soc Nephrol 29: 1706-1719, 2018.
32. Galietta LJ, Haggie PM and Verkman AS: Green fluorescent protein-based halide indicators with improved chloride and iodide affinities. FEBS Lett 499: 220-224, 2001.
33. Livak KJ and Schmittgen TD: Analysis of relative gene expression data using real-time quantitative PCR and the 2(-Delta Delta C(T)) method. Methods 25: 402-408, 2001.
34. DiCiommo DP, Duckett A, Burcescu I, Bremner R and Gallie BL: Retinoblastoma protein purification and transduction of retina and retinoblastoma cells using improved alphavirus vectors. Invest Ophthalmol Vis Sci 45: 3320-3329, 2004.
35. Procino G, Milano S, Tamma G, Dossena S, Barbieri C, Nicoletti MC, Ranieri M, Di Mise A, Nofziger C, Svelto M, *et al*: Co-regulated pendrin and aquaporin 5 expression and trafficking in Type-B intercalated cells under potassium depletion. Cell Physiol Biochem 32: 184-199, 2013.
36. Pera A, Dossena S, Rodighiero S, Gandía M, Bottà G, Meyer G, Moreno F, Nofziger C, Hernández-Chico C and Paulmichl M: Functional assessment of allelic variants in the SLC26A4 gene involved in Pendred syndrome and nonsyndromic EVA. Proc Natl Acad Sci USA 105: 18608-18613, 2008.
37. Fugazzola L, Cirello V, Dossena S, Rodighiero S, Muzza M, Castorina P, Lalatta F, Ambrosetti U, Beck-Peccoz P, Bottà G and Paulmichl M: High phenotypic intrafamilial variability in patients with Pendred syndrome and a novel duplication in the SLC26A4 gene: Clinical characterization and functional studies of the mutated SLC26A4 protein. Eur J Endocrinol 157: 331-338, 2007.
38. Dror AA, Politi Y, Shahin H, Lenz DR, Dossena S, Nofziger C, Fuchs H, Hrabé de Angelis M, Paulmichl M, Weiner S and Avraham KB: Calcium oxalate stone formation in the inner ear as a result of an Slc26a4 mutation. J Biol Chem 285: 21724-21735, 2010.
39. Dossena S, Bizhanova A, Nofziger C, Bernardinelli E, Ramsauer J, Kopp P and Paulmichl M: Identification of allelic variants of pendrin (SLC26A4) with loss and gain of function. Cell Physiol Biochem 28: 467-476, 2011.
40. Dossena S, Nofziger C, Brownstein Z, Kanaan M, Avraham KB and Paulmichl M: Functional characterization of pendrin mutations found in the Israeli and Palestinian populations. Cell Physiol Biochem 28: 477-484, 2011.
41. Bernardinelli E, Costa R, Nofziger C, Paulmichl M and Dossena S: Effect of known inhibitors of ion transport on pendrin (SLC26A4) activity in a human kidney cell line. Cell Physiol Biochem 38: 1984-1998, 2016.
42. Dossena S, Rodighiero S, Vezzoli V, Bazzini C, Sironi C, Meyer G, Fürst J, Ritter M, Garavaglia ML, Fugazzola L, *et al*: Fast fluorometric method for measuring pendrin (SLC26A4) Cl-/I-transport activity. Cell Physiol Biochem 18: 67-74, 2006.
43. Dossena S, Rodighiero S, Vezzoli V, Nofziger C, Salvioni E, Boccazzi M, Grabmayer E, Bottà G, Meyer G, Fugazzola L, *et al*: Functional characterization of wild-type and mutated pendrin (SLC26A4), the anion transporter involved in Pendred syndrome. J Mol Endocrinol 43: 93-103, 2009.
44. Tsukada K, Nishio SY, Hattori M and Usami S: Ethnic-specific spectrum of GJB2 and SLC26A4 mutations: Their origin and a literature review. Ann Otol Rhinol Laryngol 124 (Suppl 1): 61S-76S, 2015.
45. Mauthe M, Orhon I, Rocchi C, Zhou X, Luhr M, Hijlkema KJ, Coppes RP, Engedal N, Mari M and Reggiori F: Chloroquine inhibits autophagic flux by decreasing autophagosome-lysosome fusion. Autophagy 14: 1435-1455, 2018.
46. Van Goor F, Hadida S, Grootenhuis PD, Burton B, Stack JH, Straley KS, Decker CJ, Miller M, McCartney J, Olson ER, *et al*: Correction of the F508del-CFTR protein processing defect in vitro by the investigational drug VX-809. Proc Natl Acad Sci USA 108: 18843-18848, 2011.
47. Keating D, Marigowda G, Burr L, Daines C, Mall MA, McKone EF, Ramsey BW, Rowe SM, Sass LA, Tullis E, *et al*: VX-445-Tezacaftor-ivacaftor in patients with cystic fibrosis and one or two phe508del alleles. N Engl J Med 379: 1612-1620, 2018.
48. Aslam AA, Sinha IP and Southern KW: Ataluren and similar compounds (specific therapies for premature termination codon class I mutations) for cystic fibrosis. Cochrane Database Syst Rev 3: CD012040, 2023.
49. Hosoya M, Saeki T, Saegusa C, Matsunaga T, Okano H, Fujioka M and Ogawa K: Estimating the concentration of therapeutic range using disease-specific iPS cells: Low-dose rapamycin therapy for Pendred syndrome. Regen Ther 10: 54-63, 2019.
50. Dossena S, Vezzoli V, Cerutti N, Bazzini C, Tosco M, Sironi C, Rodighiero S, Meyer G, Fascio U, Fürst J, *et al*: Functional characterization of wild-type and a mutated form of SLC26A4 identified in a patient with Pendred syndrome. Cell Physiol Biochem 17: 245-256, 2006.
51. Rapid UBIquitination detection. http://old.protein.bio.unipd.it/rubi/, 2013 (accessed 5 July 2024).
52. Wang L, Hoang A, Gil-Iturbe E, Laganowsky A, Quick M and Zhou M: Mechanism of anion exchange and small-molecule inhibition of pendrin. Nat Commun 15: 346, 2024.
53. Ward CL, Omura S and Kopito RR: Degradation of CFTR by the ubiquitin-proteasome pathway. Cell 83: 121-127, 1995.
54. Chen YA, Peng YJ, Hu MC, Huang JJ, Chien YC, Wu JT, Chen TY and Tang CY: The Cullin 4A/B-DDB1-Cereblon E3 ubiquitin ligase complex mediates the degradation of CLC-1 chloride channels. Sci Rep 5: 10667, 2015.
55. Hsu PH, Ma YT, Fang YC, Huang JJ, Gan YL, Chang PT, Jow GM, Tang CY and Jeng CJ: Cullin 7 mediates proteasomal and lysosomal degradations of rat Eag1 potassium channels. Sci Rep 7: 40825, 2017.
56. Iwai C, Li P, Kurata Y, Morikawa K, Maharani N, Higaki K, Sasano T, Notsu T, Ishido Y, Miake J, *et al*: Hsp90 prevents interaction between CHIP and HERG proteins to facilitate maturation of wild-type and mutant HERG proteins. Cardiovasc Res 100: 520-528, 2013.
57. Gozzetti A, Papini G, Candi V, Brambilla CZ, Sirianni S and Bocchia M: Second generation proteasome inhibitors in multiple myeloma. Anticancer Agents Med Chem 17: 920-926, 2017.
58. Zeniya M, Mori T, Yui N, Nomura N, Mandai S, Isobe K, Chiga M, Sohara E, Rai T and Uchida S: The proteasome inhibitor bortezomib attenuates renal fibrosis in mice via the suppression of TGF-β1. Sci Rep 7: 13086, 2017.
59. Ikeda T, Fujii H, Nose M, Kamogawa Y, Shirai T, Shirota Y, Ishii T and Harigae H: Bortezomib treatment induces a higher mortality rate in lupus model mice with a higher disease activity. Arthritis Res Ther 19: 187, 2017.
60. Pohl C and Dikic I: Cellular quality control by the ubiquitin-proteasome system and autophagy. Science 366: 818-822, 2019.
61. Sheridan C: Drug makers target ubiquitin proteasome pathway anew. Nat Biotechnol 33: 1115-1117, 2015.
62. Sarikas A, Hartmann T and Pan ZQ: The cullin protein family. Genome Biol 12: 220, 2011.
63. Bulatov E and Ciulli A: Targeting Cullin-RING E3 ubiquitin ligases for drug discovery: Structure, assembly and small-molecule modulation. Biochem J 467: 365-386, 2015.

64. Guedat P and Colland F: Patented small molecule inhibitors in the ubiquitin proteasome system. BMC Biochem 8 (Suppl 1): S14, 2007.
65. Landre V, Rotblat B, Melino S, Bernassola F and Melino G: Screening for E3-ubiquitin ligase inhibitors: Challenges and opportunities. Oncotarget 5: 7988-8013, 2014.
66. Younger JM, Chen L, Ren HY, Rosser MF, Turnbull EL, Fan CY, Patterson C and Cyr DM: Sequential quality-control checkpoints triage misfolded cystic fibrosis transmembrane conductance regulator. Cell 126: 571-582, 2006.
67. Liu J, Ye J, Zou X, Xu Z, Feng Y, Zou X, Chen Z, Li Y and Cang Y: CRL4A(CRBN) E3 ubiquitin ligase restricts BK channel activity and prevents epileptogenesis. Nat Commun 5: 3924, 2014.
68. Mijnders M, Kleizen B and Braakman I: Correcting CFTR folding defects by small-molecule correctors to cure cystic fibrosis. Curr Opin Pharmacol 34: 83-90, 2017.
69. Tomati V, Sondo E, Armirotti A, Caci E, Pesce E, Marini M, Gianotti A, Jeon YJ, Cilli M, Pistorio A, *et al*: Genetic inhibition of the ubiquitin ligase Rnf5 attenuates phenotypes associated to F508del cystic fibrosis mutation. Sci Rep 5: 12138, 2015.
70. Sondo E, Falchi F, Caci E, Ferrera L, Giacomini E, Pesce E, Tomati V, Mandrup Bertozzi S, Goldoni L, Armirotti A, *et al*: Pharmacological inhibition of the ubiquitin ligase RNF5 rescues F508del-CFTR in cystic fibrosis airway epithelia. Cell Chem Biol 25: 891-905.e8, 2018.

Copyright © 2025 Bernardinelli et al. This work is licensed under a Creative Commons Attribution-NonCommercial-NoDerivatives 4.0 International (CC BY-NC-ND 4.0) License.